J Infrared Milli Terahz Waves (2018) 39:546–552
https://doi.org/10.1007/s10762-018-0479-1

A Millimetre-Wave Cuboid Solid Immersion Lens with Intensity-Enhanced Amplitude Mask Apodization

Liyang Yue[1] · Bing Yan[1] · James N. Monks[1] · Rakesh Dhama[1] · Zengbo Wang[1] · Oleg V. Minin[2] · Igor V. Minin[3]

Received: 24 October 2017 / Accepted: 6 March 2018 /
Published online: 15 March 2018

Abstract Photonic jet is a narrow, highly intensive, weak-diverging beam propagating into a background medium and can be produced by a cuboid solid immersion lens (SIL) in both transmission and reflection modes. Amplitude mask apodization is an optical method to further improve the spatial resolution of a SIL imaging system via reduction of waist size of photonic jet, but always leading to intensity loss due to central masking of the incoming plane wave. In this letter, we report a particularly sized millimetre-wave cuboid SIL with the intensity-enhanced amplitude mask apodization for the first time. It is able to simultaneously deliver extra intensity enhancement and waist narrowing to the produced photonic jet. Both numerical simulation and experimental verification of the intensity-enhanced apodization effect are demonstrated using a copper-masked Teflon cuboid SIL with 22-mm side length under radiation of a plane wave with 8-mm wavelength. Peak intensity enhancement and the lateral resolution of the optical system increase by about 36.0% and 36.4% in this approach, respectively.

Keywords Solid immersion lens · Apodization · Photonic jet · Cuboid lens · Millimetre-wave

1 Introduction

The Abbe criterion defines that the optical resolution is limited at $\lambda/2$ for an imaging system with a numerical aperture (NA) equalling to 1 when its light collection reaches a solid angle of

✉ Liyang Yue
l.yue@bangor.ac.uk

✉ Igor V. Minin
prof.minin@gmail.com

[1] School of Electronic Engineering, Bangor University, Dean Street, Bangor LL57 1UT Gwynedd, UK

[2] National Research Tomsk State University, Lenin Ave., 36, Tomsk 634050, Russia

[3] National Research Tomsk Polytechnic University, Lenin Ave., 30, Tomsk 634050, Russia

2π [1]. A near-field SIL whose object space is filled by a high-refractive-index solid material can advance the spatial resolution to a sub-wavelength volume due to its higher NA than that of normal far-field objective lens [2]. Here, the NA enhancement factor is the refractive index, n, of the SIL material which replaces the air to scatter the incident rays [3, 4]. Consequently, an elongate, narrow and high intensive focusing region, known as the photonic jet, is formed in the near-field of scattering of the plane wave radiation by SIL shadow-side [5]. Refractive index contrast (SIL material to background medium) and scale effect (SIL size to wavelength) are considered as two main factors that form the photonic jet [6, 7]. Scale effect can influence the phase delay along the wave front, which causes position change of the produced photonic jet. In 1990, Mansfield et al. firstly used a confocal microscope equipped SIL to resolve 100-nm lines and spaces [8]. Subsequently applications of SIL in photolithography and data storage were well studied by Corle et al. [9] and Terris et al. [10], respectively.

A variety of methods, including use of the new high-index materials and the innovative structure arrangements, were attempted to lift resolution of a SIL to a super-resolution level for the important applications in imaging and sensing these years [11–14]; however, high material cost and harsh control conditions restrict their operations on a wide range of imaging/sensing targets. By contrast, the amplitude mask apodization accomplished by adding a pupil mask on a SIL was found to be a relatively easy procedure to optimise the resolution of a near-field optical system through waist narrowing (reduction of the full width at half maximum, FWHM) of a photonic jet [15–17]. Nevertheless, intensity loss is always unavoidable in the system applied by this method, because the centred pupil mask lowers the amount of the incoming rays to be admitted in the SIL. For this reason, the amplitude mask apodization was considered as a method that only is adequate for an optical system with the sufficient optical energy efficiency for a long time [18, 19].

Knowledge about intensity loss in amplitude mask apodization was challenged in 2017. Yue et al. simulated focusing of a cuboid fused silica particle lens and concluded that the produced photonic jet may have a higher peak field intensity than that in the non-pupil-masked case [20]. Compared with the same sized spherical particle lens or other particle lenses with the arbitrary shapes, cuboid particle lens or SIL commonly stimulates a longer photonic jet with a more circular profile in the radial direction [21], and the corresponding focusing properties in THz band were investigated in the previous publications [22, 23]. In this letter, we experimentally verified the effect of anomalous amplitude mask apodization that simultaneously delivers intensity enhancement and focus narrowing to the photonic jet in millimetre band for the first time, which is also a successful validation of scale effect for our previous simulation of the pupil-masked SIL functioning in the optical band. A model of a copper-masked Teflon (Polytetrafluoroethylene, PTFE) cuboid SIL with 22-mm side length was initially created by using the finite element method (FEM) to simulate the near-field E^2 field intensity distribution under a plane wave radiation of 8-mm wavelength (37.5 GHz). Subsequently, a physical substance of a SIL according to the modelling conditions was fabricated, and E^2 field intensity and near-field patterns of the photonic jet by it were measured as the focusing and frequency properties of the quasi-optics at the different scanning angles.

2 Results and Discussion

Numerical model of the cuboid SIL was built in the commercial FEM software package—CST Microwave Studio©. A plane wave of 8-mm wavelength (λ) equalling to 37.5 GHz frequency

propagates from $+z$ to $-z$ direction with a polarisation along y axis which is vertical to the optical bench in the experiment. Optical properties—refractive index, n, and extinction coefficient, k, for Teflon ($n = 1.43$, $k = 1.4 \times 10^{-4}$) and copper ($n = 0.88$, $k = 11.70$)—are based on the previous literatures [24–27]. Diagram of the experimental setup is shown in Fig. 1a. Based on the conditions of our fabrication and measurement equipment and the numerous simulations of focusing of Teflon SIL with multiple sizes, side length, L, of 22 mm equalling 2.75λ is selected as the dimension of the cuboid SIL to demonstrate the aforementioned unique performance. A piece of Teflon bulk material was cut into a cuboid SIL of that size by machining on a lathe holding tolerance as small as 0.05 mm for the experiment, and a square-shaped copper foil with 11-mm side length ($L/2$) and 0.2-mm thickness was placed at the centre of the face encountering a plane wave to perform amplitude mask apodization, as shown in inset in Fig. 1a. A backward-wave tube (BWT) was used as a source of millimetre-wave radiation. Radiation was inputted into a cymometer through a coupler to calibrate the working frequency of the BWT. A D-407 type diode was coupled with the tapered dielectric rod waveguide (DRW) antenna to measure the received power [28], which is recorded to a selective nanovoltmeter. Independently, a tapered rectangular waveguide probe with a slit aperture was also used (Results measured by these two near-field probes were identical) [29]. The output of BWT was guided to a pin-diode waveguide modulator with a cut-off coefficient of 10^5 via an attenuator. The modulation frequency was imposed to 1 kHz by a G6-15 generator. Also, frequency control was attained by monitoring the voltage at the retarding system of BWT using a digital voltmeter. A signal generator placed in a far-field distance—300 mm—illuminated the slow-diverging quasi-flat wave front to the cuboid SIL fixed in a through hole with 44-mm diameter on an absorption screen. The measured amplitude distribution of the collimator in x direction is shown in the Fig. 1b. The unevenness of the amplitude distribution does not exceed 0.3 dB in the cuboid SIL space ranged from $x/L = -0.3$ to $x/L = 0.7$ with the coordinate normalised to the side length (L). Besides, focusing

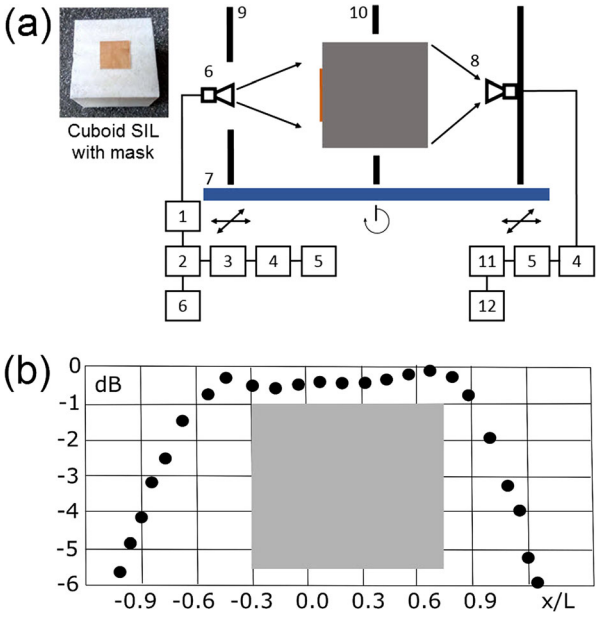

Fig. 1 (**a**) Experimental setup: 1 attenuator, 2 directional coupler, 3 wave meter, 4 millimetre-wave receiver, 5 selective nanovoltmeter, 6 signal generator, 7 optical bench, 8 open end of waveguide with DRW, 9 protection shields, 10 cuboid SIL, 11 digital recording oscilloscope and 12 continuous recording plotter. The distance between the 6 source and 10 cuboid SIL corresponds to the conditions of far-field. Left inset: a fabricated Teflon cuboid SIL with copper mask. (**b**) The measured amplitude distribution of the collimator in x direction. The cuboid SIL occupies the space from $x/L = -0.3$ to $x/L = 0.7$ indicated by a grey-colour area

of a non-masked cuboid SIL was also simulated and experimentally measured for comparison. Techniques of construction and measurement in this experiment were introduced in detail in the paper [30].

The simulated distributions of near-field E^2 field intensity (Absolute value field component with amplitude complex field vector) on xz plane are illustrated in Fig. 2a, b for the masked and non-masked cases, respectively. Only the xz plane as the plane with the shortest FWHM is demonstrated to emphasise the intensity enhancement and waist narrowing of the photonic jet induced by the cuboid SIL with mask apodization. Photonic jet in the yz plane has the similar shape as shown in Fig. 2, but waist is wider. Figure 2a shows that the cuboid SIL without amplitude mask apodization produces a main photonic jet along the central axis and two less-intense jets by its sides. Meanwhile, in Fig. 2b, a single narrower photonic jet generated by the masked cuboid SIL creates a much stronger intensity enhancement near the shadow surface of the SIL than that shown in the non-masked case. Maximum values of E^2 field intensity are 17.3 and 12.7 for the models with and without amplitude mask apodization respectively, which means about 36.2% enhancement is predicted from the simulation.

Also, Fig. 3a, b demonstrates the simulated and experimentally measured profiles of E^2 field intensity passing the focus (positions where maximum E^2 field intensities are at) along z and x directions, respectively. Maximum value of E^2 field intensity shown in each figure is normalised to 1.0 to refer the relative positions for the simulation results and the absolute measurements in experiment. Plane wave propagates from left to right in '-' direction as shown by a red arrow in Fig. 3a. Cuboid SIL is settled from the position 0 to −22 on z axis, and its volume representing as the side length of 22 mm is denoted by an area between a black dashed line and the axis of ordinates in Fig. 3a. Maximum E^2 field intensity is experimentally measured to increase by 35.7% with amplitude mask apodization. This figure is slightly lower than the prediction of 36.2% in simulation. Meanwhile, it is found that the measured E^2 field intensity in the masked case (black square markers) drops more quickly after the peak value than those in the non-masked case (red circle markers), as shown in Fig. 3a, which is in

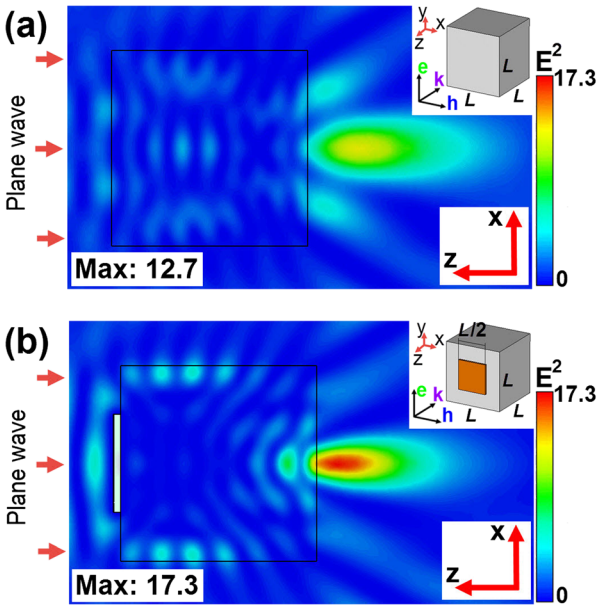

Fig. 2 Simulated near-field E^2 field enhancement distribution on xz plane (**a**) without and (**b**) with the amplitude mask apodization

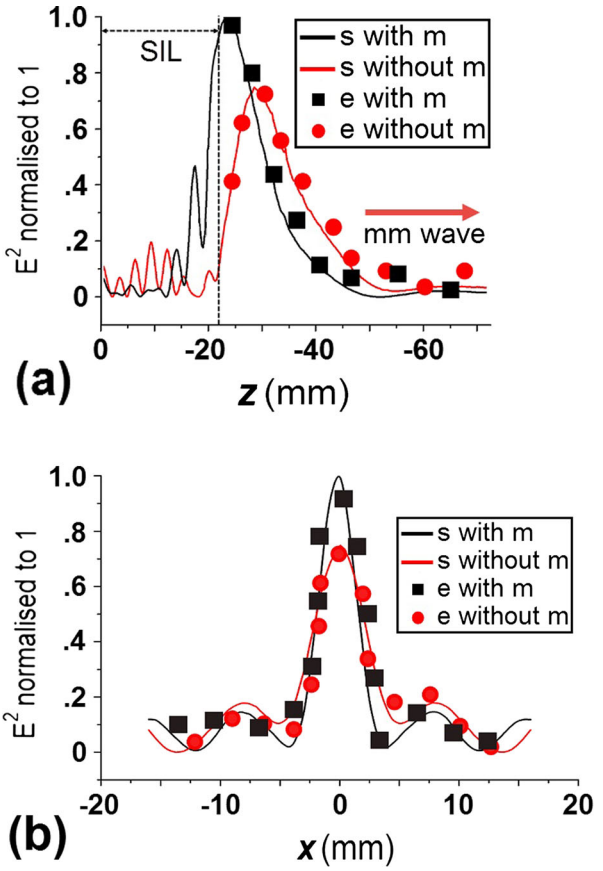

Fig. 3 The simulated and experimentally measured profiles of E^2 field enhancement passing the focus (**a**) at $x = 0$ mm, $y = 0$ mm along the z direction and (**b**) at $y = 0$ mm, $z = -25$ mm (masked case) and $z = -31$ mm (non-masked case) in the x direction; s: simulation, e: experiment, m mask

accordance with a shorter photonic jet caused by amplitude mask apodization in the simulation illustrated in Fig. 2b.

In Fig. 3b, the measured x direction profiles (markers) passing the focus on z axis ($z = -25$ mm in the masked case, and $z = -31$ mm in the non-masked case in Fig. 3a) ideally reflect the waist size reduction of the produced photonic jet after amplitude mask apodization. FWHMs obtained from the numerical simulation and experimental measurement are very close, representing as about 5.20 mm for the case without mask apodization and about 3.31 mm for the case with mask apodization, respectively. About 36.4% shortening of the FWHM is realised by both approaches. Accuracy estimation of the experimentally measured FWHMs is 0.1 mm (about ± 2.5%), which is limited by the positioning error of the mechanically driven detector we use. Thus, Fig. 3 manifests that the measured values of E^2 field intensity (markers) well fit the trend of the corresponding simulation values (solid line curves), which means that key features of the intensity-enhanced amplitude mask apodization on the cuboid SIL, including increase of the maximum field intensity, waist reduction and length shortening, are experimentally verified.

According to the measured data and near-field simulation of E^2 field intensity, as shown in Figs. 2 and 3, we determine that mechanism of the intensity-enhanced amplitude mask apodization depends on characteristics of formation of a photonic jet by a cuboid SIL and the related influence from the central screening. In fact, formation of a photonic jet by a

non-spherical particle lens is attributed to phase delay introduced by diffraction along the wave front [31], rather than the refraction in the geometrical optics for a scenario using a spherical or cylindrical particle lens [16]. For this reason, a pupil mask centred on the face encountering the plane wave may not break the geometrical integrity of cuboid in the focusing process. This break normally happens in the spherical particle lens to result in intensity loss of the photonic jet [16]. Besides, amplitude mask apodization increases the NA of the cuboid SIL [20], and our measurement precisely detects the consequent focus movement towards the SIL shadow surface, as shown in Fig. 3a. The corresponding shifting of the focus shortens the propagation distance of the wave in the background medium, moreover strengthens convergence of the wave power that just exits from the lower boundary of the cuboid SIL, as shown in Fig. 2b.

3 Conclusion

We use an experiment to confirm the simulation-predicted [19] effect of the anomalous intensity-enhanced amplitude mask apodization, which simultaneously increases maximum E^2 field intensity and resolution beyond the diffraction limit near the shadow surface of a cuboid dielectric SIL. This phenomenon is different from the normally reported intensity loss caused by amplitude mask apodization for the spherical SIL. Its key features, e.g. growth of maximum field intensity, shortening of jet length and waist size, are experimentally demonstrated via measurement of E^2 field intensity profiles passing the focus. This phenomenon may possess the scale effect and would be valid in multiple frequency bands, including the optical band.

Funding Information This work received financial support from the Sêr Cymru National Research Network in Advanced Engineering and Materials (NRNF66 and NRN113), Wales, UK, the Knowledge Economy Skills Scholarships (KESS 2, BUK289), Wales, UK, Tomsk Polytechnic University Competitiveness Enhancement Program grant, Russia, and Mendeleev scientific fund of Tomsk State University, Russia.

References

1. S. G. Lipson, H. Lipson, and D. S. Tannhauser, Optical Physics (Cambridge University Press, Cambridge, 1998).
2. A. N. Vamivakas, R. D. Younger, B. B. Goldberg, A. K. Swan, M. S. Ünlü, E. R. Behringer, Am. J. Phys. **76**, 758 (2008).
3. S. Y. Yim, J. H. Kim, J. Lee, J. Opt. Soc. Korea **15**, 78–81 (2011).
4. N.V. Chernomyrdin, A.O. Schadko, S.P. Lebedev, V.L. Tolstoguzov, V.N. Kurlov, I.V. Reshetov, I.E. Spektor, M. Skorobogatiy, S.O. Yurchenko, K.I. Zaytsev, Applied Physics Letters **110** (22), 221109 (2017)
5. D. McCloskey, J. J. Wang, J. F. Donegan, Opt. Express **20**, 128–140 (2012).
6. B. S. Luk'yanchuk, R. Paniagua-Dominguez, I. V. Minin, O. V. Minin, Z. B. Wang, Opt. Mater. Express **7**, 1820–1847 (2017).
7. I. V. Minin, and O. V. Minin, Diffractive Optics and Nanophotonics: Resolution Below the Diffraction Limit (Springer, Berlin, 2016).
8. S. M. Mansfield, G. S. Kino, Appl. Phys. Lett. **57**, 2615 (1990).
9. T. R. Corle, G. S. Kino, S. M. Mansfield, U.S. Patent, US5121256 A (1992).
10. B. D. Terris, H. J. Mamin, D. Rugar, Appl. Phys. Lett. **65**, 388 (1994).
11. W. Fan, B. Yan, Z. B. Wang, L. Wu, Sci. Adv. **2**, e1600901 (2016).
12. L. Yue, B. Yan, Z. B. Wang, Opt. Lett. **41**, 1336–1339 (2016).
13. C. M. Soukoulis, M. Wegener, Nat. Photonics **5**, 523–530 (2011).
14. I.N. Dolganova, K.I. Zaytsev, A.A. Metelkina,V.E. Karasik, S.O. Yurchenko, Review of Scientific Instruments **86** (11), 113704 (2015).

15. I. V. Minin, O. V. Minin, Patent of Russia 153686 (2015).
16. B. Yan, L. Yue, Z. B. Wang, Opt. Commun. **370**, 140–144 (2016).
17. M. Wu, R. Chen, J. Soh, Y. Shen, L. Jiao, J. Wu, X. Chen, R. Ji, M. Hong, Sci. Rep. **6**, 31637 (2016).
18. H. Luo, C. Zhou, Appl. Opt. **43**, 6242–6247 (2004).
19. M. Yun, M. Wang, L. Liu, J. Opt. A: Pure Appl. Opt. **7**, 640 (2005).
20. L. Yue, B. Yan, J. N. Monks, Z. B. Wang, N. T. Tung, V. D. Lam, O. V. Minin, I. V. Minin, J. Phys. D: Appl. Phys. **50**, 175102 (2017).
21. Y. E. Geints, I. V. Minin, E. K. Panina, A. A. Zemlyanov, O. V. Minin, Opt. Quant. Electron. **49**, 118 (2017).
22. V. Pacheco-Peña, M. Beruete, I. V. Minin, O. V. Minin, Appl. Phys. Lett. **105**, 084102 (2014).
23. H. H. Nguyen Pham, S. Hisatake, I. V. Minin, O. V. Minin, T. Nagatsuma, Appl. Phys. Lett. **108**, 191102 (2016).
24. V. E. Lyubchenko, Science and Technology of Millimetre Wave Components and Devices (CRC press, Boca Raton, 2001).
25. A. Elhawil, L. Zhang, J. Stiens, C. De Tandt, N. A. Gotzen, G. V. Assche, and R. Vounckx, A quasi-optical free-space method for dielectric constant characterization of polymer materials in mm-wave band (Proceedings Symposium IEEE/LEOS Benelux Chapter, Brussels, 2007).
26. H. J. Hagemann, W. Gudat, C. Kunz, J. Opt. Soc. Am. **65**, 742–744 (1975).
27. H. J. Hagemann, W. Gudat, C. Kunz. DESY report SR-74/7 (1974).
28. W. G. Kim, J. P. Thakur, Y.H. Kim, Microwave Opt. Technol. Lett. **52**, 1221 (2010).
29. T. Nozokido, J. Bae, K. Mizuno, IEEE Trans. on Microwave Theory and Techn. **49**, 491–499 (2001).
30. I. V. Minin, O. V. Minin, Microwave Opt. Technol. Lett. **56**, 2436–2439 (2014).
31. I. V. Minin, O. V. Minin, Y. Geintz, Ann. Phys. (Berlin) **527**, 491 (2015).